PROCEEDINGS, Fourtieth Workshop on Geothermal Reservoir Engineering
Stanford University, Stanford, California, January 26-28, 2015
SGP-TR-204

Simulation of Proppant Transport in 2D Discrete Fracture Network

Sogo Shiozawa, Mark McClure

The University of Texas at Austin

200 E. Dean Keeton, Austin, TX 78712

sogo@utexas.edu; mcclure@austin.utexas.edu

Keywords: proppant transport, discrete fracture network, EGS

ABSTRACT

We developed a modeling approach to describe proppant transport in two-dimensional discrete fracture networks models. We implemented our approach into the two-dimensional version of the discrete fracture network (DFN) simulator Complex Fracturing ReseArch Code (CFRAC). Conventionally, proppant is not used in Enhanced Geothermal Systems (EGS), though it is widely used in hydraulic fracturing for hydrocarbon recovery. It is believed in the EGS community that slip on preexisting fractures (shear stimulation) is the only important mechanism of stimulation and so proppant is not necessary. In this paper, based on the idea that newly forming hydraulic fractures can propagate and play a key role in EGS, we discuss proppant transport in natural and hydraulic fractures and its impact on stress, aperture, and transmissivity. To model the process of proppant settling with a two-dimensional model, we split each fracture element into two sections: a proppant bed at the bottom of the fracture and a slurry (mixture of fluid and proppant) above the proppant bed. The model takes into account fracture closure around the proppant and the effect of closure on fracture properties. The results demonstrate that our formulation can describe proppant transport, proppant settling, proppant erosion, and fracture closure in a fully consistent way.

1. INTRODUCTION

Proppant is solid particulate matter, most often sand or ceramic material, injected during hydraulic fracturing treatments to hold fractures open and allow them to maintain transmissivity after the end of injection. In the hydrocarbon industry, successful proppant placement is considered critical for long term enhancement of production. However, proppant has rarely been used in the geothermal industry because it is generally believed that unpropped fractures should have adequate transmissivity to sustain production (McClure and Horne, 2014). Nevertheless, inability to achieve high fracture transmissivity remains a major challenge for EGS. Shiozawa and McClure (2014) and Li et al. (2014) suggested EGS design with horizontal wells, multiple stages, and proppant based on the idea that propped hydraulic fractures can play an important role in EGS.

Most computational approaches to proppant transport are implemented in three-dimensional hydraulic fracturing simulators. However, it would be useful to model proppant transport in two-dimensional models, because they are more efficient, especially when simulating very large fracture networks. But gravitational settling of proppant is an important physical process, especially when relatively low viscosity fluid is used, and this is difficult to incorporate into a two-dimensional model.

We developed and implemented a method for proppant transport modeling in two-dimensional discrete fracture networks. The model divides fracture elements into two sections: slurry and proppant bed. The proppant bed forms due to gravitational settling of proppant out of the slurry. The model also accounts for erosion and fracture closure.

2. METHODOLOGY

To perform proppant transport modeling, modifications were made to an existing code, CFRAC (Complex Fracturing ReseArch Code), which was developed by McClure and Horne (2013). CFRAC is a two-dimensional discrete fracture network simulator which calculates fluid pressure, fracture sliding, fracture opening, and the stresses induced by fracture deformation. During each time step, shear traction boundary conditions, unsteady state fluid mass balance, and boundary conditions involving normal stress are solved simultaneously and implicitly. The stresses induced by deformation are calculated with the boundary element method (Displacement Discontinuity Method) proposed by Shou and Crouch (1995). For this study, we added two additional mass balance equations: unsteady state mass balance equations for proppant in the slurry and the proppant bed. The new variables are proppant mass concentration in the slurry and proppant bed height. The fluid mass balance equation had to be modified to account for the effect of entrained proppant in the slurry.

2.1 The original version of CFRAC

In this section, the equations solved by the original version of CFRAC are introduced. The details of the equations and numerical implementation are shown in other publications (McClure, 2012: McClure and Horne, 2013).

In finite volume form, the unsteady state fluid mass balance equation is:

$$\frac{\partial\left(2ahE\rho_f\right)}{\partial t} = -\sum f - q_{leakoff} + s\,, \tag{1}$$

$$f = -T\frac{\rho_f}{\mu_f}dP\,, \tag{2}$$

where E is fracture void aperture, a is element half-length, h is element height, ρ_f is fluid density, t is time, f is the mass flow rate into or out of a fracture element, T is the fracture transmissibility (related to hydraulic aperture e, through the cubic law and also accounting for element geometry), $q_{leakoff}$ is the mass rate of leakoff per fracture surface area into the surrounding matrix, s is a source term representing a well, μ_f is fluid viscosity, and dP is fluid pressure difference between two elements. Nonlinear constitutive laws are used to relate fracture aperture to fluid pressure, aperture, and cumulative sliding displacement.

Fracture elements are defined as closed if their fluid pressure is less than their normal stress. For closed elements, the Coulomb failure criterion with a radiation damping term is enforced (Jaeger et al., 2007):

$$\left|\tau - \eta v\right| = \mu_f \sigma_n^{'} - S_0\,, \tag{3}$$

where τ is shear stress, ηv is the radiation damping term (Rice, 1993), S_0 is fracture cohesion and σ_n' is the effective normal stress, defined as (Jaeger et al., 2007):

$$\sigma_n^{'} = \sigma_n - P\,. \tag{4}$$

If the shear stress is less than the frictional resistance to slip, as given by Equation 3, the fracture is assumed to be not sliding.

Fractures are considered open when the fluid pressure exceeds their normal stress and the fracture walls come out of contact. When a fracture is open, the effective normal stress is enforced to be equal to zero (Crouch and Starfield, 1983).

$$\sigma_n^{'} = 0\,. \tag{5}$$

Also, the shear stress on open fractures is enforced to be equal to zero:

$$\left|\tau - \eta v\right| = 0\,. \tag{6}$$

These equations are solved to calculate the sliding and opening displacement and the fluid pressure. The fluid is assumed to be single phase and isothermal. A three-dimensional version of CFRAC has been developed (McClure et al., 2015), but this paper is focused on implementing proppant transport in the 2D code.

2.2 Modeling of proppant transport

There is an extensive literature on proppant transport modeling (Mobbs and Hammond, 2001; Gadde et al., 2004; Dontsov and Peirce, 2014). Typically, the formation of a proppant bed and fracture closure are not handled.

2.2.1 Assumptions

The model assumes that proppant consists of spherical grains and all the grains have a same density and size. The model also assumes that the proppant is incompressible (the shape does not change and its density is constant), that the fracture has a fixed height, and that the pressure gradient in the vertical direction is zero so that there is only a pressure gradient along the fracture.

The fracture can be conceptualized as containing three zones: a proppant free zone, a slurry zone, and a proppant packed bed zone (Wang et al., 2003). In this study, we neglected the proppant free zone and modeled the fracture as containing a backed bed and an overlying slurry zone. Slurry is the mixture of frac fluid and proppant, and is assumed to have uniform concentration within an element. The proppant bed forms at the bottom of the fracture due to gravitational settling. The proppant bed height is assumed constant within each element.

Three mass balance equations are solved: proppant in the slurry, proppant in the bed, and fluid (in both the slurry and the bed). Fluid flow occurs through both the slurry region and the packed bed. The proppant can only flow along the fracture within the slurry phase. There is no proppant transport within the bed. The proppant bed changes height in each element as proppant is either eroded or deposited, creating mass transfer of proppant between the slurry and bed within each individual element. Figure 1 schematically shows the concept of our model.

The rate of deposition/erosion is related to the equilibrium bed height. The equilibrium bed height is calculated from the correlation given by Wang et al. (2003). We assumed an arctangent relationship to describe how quickly proppant can erode or deposit, as the bed evolves over time to reach the equilibrium bed height, as described in Section 2.2.3.

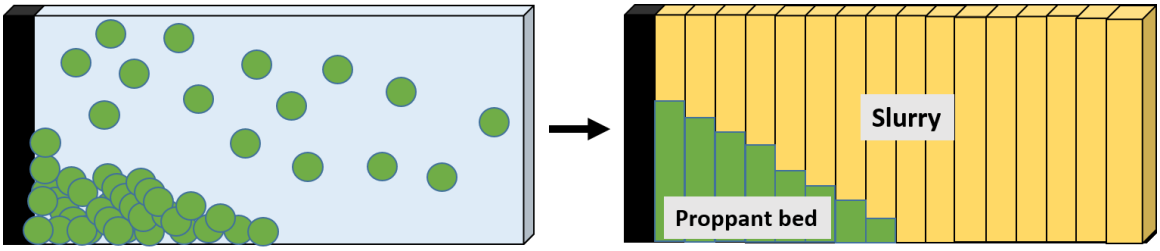

Figure 1: Two-section model of proppant transport. The black line is the wellbore and the other rectangles represent fracture elements.

2.2.2 Mass balance equation of proppant

In finite volume form, the unsteady state mass balance equations on proppant in slurry (7-a), proppant in the wellbore (7-b), and proppant in the bed (8) are:

$$\frac{\partial\left(2aC_s\left(h-h_b\right)E_{upper}\right)}{\partial t}=-\sum f-NDE\,, \tag{7-a}$$

$$\frac{\partial\left(V_{well}C_s\right)}{\partial t}=-\sum f+q_s\,, \tag{7-b}$$

$$\frac{\partial\left(2ah_bE_b\left(1-\phi_b\right)\rho_p\right)}{\partial t}=NDE\,, \tag{8}$$

where a is the half-length of fracture elements, C_s is the proppant mass concentration, h is the fracture height (constant), h_b is the proppant bed height, E_{upper} is aperture above the proppant bed, f is mass flow rate of proppant, NDE (the net deposition/erosion term) is mass rate of proppant into/out of proppant bed, V_{well} is the volume of wellbores, q_s is the injection/production rate of proppant, E_b is the thickness of proppant bed, and $\phi_b$is the porosity of proppant bed.

The porosity of the proppant bed is given as:

$$\phi_b=\phi_{b,\max}\ \text{(for open elements)}, \tag{9}$$

$$\phi_b=\phi_{b,\max}\exp\left(C_{\phi_b}\left(\sigma_n-P\right)\right)\ \text{(for closed elements)}, \tag{10}$$

where $\phi_{b,max}$ is the maximum porosity of proppant bed, C_{ϕ_b} is the porosity compressibility. The mass flow rate of proppant between the slurry region of two elements is given as:

$$f=-\frac{C_sT_sdP}{\mu_s}\,, \tag{11}$$

where T_s is the transmissibility of the slurry section of the fracture, and μ_s is the slurry viscosity. The slurry viscosity is calculated with the following equation (Adachi et al., 2007):

$$\mu_s=\mu_f\left(1-\frac{C_s}{\rho_pC^*}\right)^{\beta}\,, \tag{12}$$

where C^* is the saturation concentration, usually given by 0.52 and $\beta$is a constant between -3 and -1.

2.2.3 Net erosion/deposition term

The net deposition/erosion term is given as:

$$NDE=\frac{q_d}{2}\left[\arctan\left(\frac{h_{equil}-h_b-h_{b0}}{B}\right)\frac{2}{\pi}+1\right]-\frac{q_e}{2}\left[\arctan\left(\frac{-h_{equil}+h_b+h_{b0}}{B}\right)\frac{2}{\pi}+1\right], \tag{13}$$

$$q_d=2aEv_sC_s\,, \tag{14}$$

$$q_e=2aEv_s\left(1-\phi_b\right)\rho_p\,, \tag{15}$$

where q_d is the mass deposition rate, q_e is the mass erosion rate, v_s is the settling velocity of proppant (vertical direction), h_{equil} is the equilibrium height of proppant, and B is a constant. The equilibrium height is calculated by the empirical equation shown by Wang et al (2003). The settling velocity changes depending on Reynolds number (Section 2.2.4). We use the same velocity for both deposition and erosion, v_s, although they can be specified to be different.

Equation 13 was used in order to enforce that the NDE term is a continuous function, ensuring that problem variables change gradually in time and guaranteeing convergence can be achieved by reducing timestep duration. Figure 2 shows the behavior of NDE term as a function of the difference between the equilibrium height and proppant bed height. The NDE term goes to zero as the difference between h_b and h_{equil} goes to zero. As the difference becomes far from zero, the NDE term approaches a constant value. In the schematic, the maximum deposition rate is 10 kg/s and the maximum erosion rate is 20 kg/s.

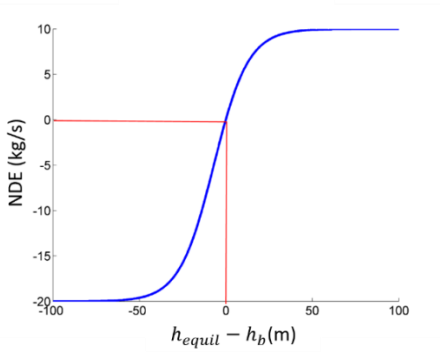

Figure 2: The behavior of the NDE term.

2.2.4 Settling velocity of proppant

The settling velocity of proppant changes depending on Reynolds number, defined as (Mack et al., 2014):

$$\mathrm{Re} = \frac{d v_s \rho_f}{\mu_f}. \tag{16}$$

For low Reynold numbers, the settling velocity is given from Stokes' law by:

$$v_s = \frac{g\left(\rho_p - \rho_f\right) d^2}{18\mu_f} \quad (\mathrm{Re} < 2). \tag{17-a}$$

For intermediate and high Reynolds numbers, they are:

$$v_s = \left[\frac{0.072 g\left(\rho_p - \rho_f\right) d^{1.6}}{\rho_f^{0.4} \mu_f^{0.6}}\right]^{0.71} \quad (2 < \mathrm{Re} < 500), \tag{17-b}$$

$$v_s = 1.74\sqrt{\frac{g\left(\rho_p - \rho_f\right) d}{\rho_f}} \quad (500 < \mathrm{Re} < 200{,}000), \tag{17-c}$$

where g is the gravitational acceleration and d is proppant diameter. This may cause discontinuity in the simulation when fluid density and viscosity are variables. This issue will be handled as future work.

When the proppant concentration is extremely high (more than 10 lb/gal or 1198.26 kg/m^3), the settling of proppant is hindered (McGhee 1991), and given as:

$$v_{s,hindered} = v_s\left(1 - \frac{C_s}{\rho_p}\right)^{4.65}. \tag{18}$$

2.2.5 Modification to the fluid mass balance equation

The fluid mass balance equations were modified to account for the presence of proppant and to account for fluid storage and flow in both the proppant bed and the slurry region. The following two equations provide the fluid mass balance for fracture elements, and the wellbore, respectively.

$$\frac{\partial\left(\rho_f\left[h_b\phi_b E_b+\left(h-h_b\right)E\left(1-V_{fs}\right)\right]\right)}{\partial t}=-\sum\left[\frac{T_b}{\mu_f}+\frac{T_s\left(1-V_{fs}\right)}{\mu_s}\right]\rho_f dP-q_{leakoff}+s\,, \tag{19}$$

$$\frac{\partial\left(V_{well}\rho_f\left(1-V_{fs}\right)\right)}{\partial t}=-\sum\left[\frac{T_b}{\mu_f}+\frac{T_s\left(1-V_{fs}\right)}{\mu_s}\right]\rho_f dP+q_f\,, \tag{20}$$

where E_b is the thickness of proppant bed, V_{fs} is the volume fraction of proppant in slurry, T_b and T_s are transmissivity of proppant bed and slurry, respectively, and q_f is fluid injection rate at the surface.

2.2.6 Solving the coupled system

The system of nonlinear equations is solved using an iterative method with iterative coupling between (1) the shear traction equations (Equations 3 and 6), (2) the flow and normal traction equations (Equations 18, 19, and 5), and (3) the proppant mass balance equations (Equations 7 and 8). The method used in this paper is an extension of the method described by McClure and Horne (2013). In an iterative coupling scheme, systems of equations are solved sequentially, and the process is repeated until all equations are simultaneously satisfied (Kim et al., 2011). Figure 3 shows the summary of the iterative coupling approach for a single time step.

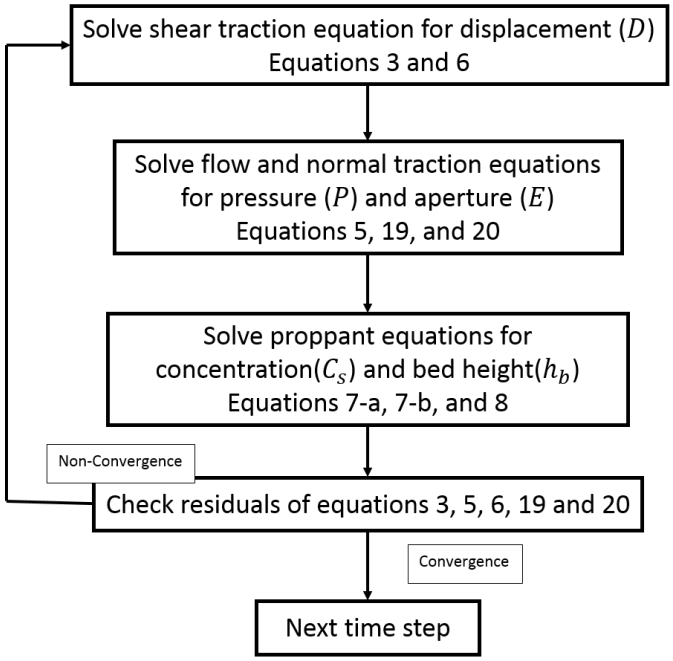

Figure 3: Summary of the iterative coupling approach for a single time step.

Within each system of equations, an iterative scheme is used. An iteration matrix *J* is formed, where the *i*th row and *j*th column is given as:

$$J_{ij}=\frac{\partial Ri}{\partial Xj}\,, \tag{21}$$

where *R* is the vector of residual equations (equal to zero if the equations are perfectly satisfied) and *X* is the vector of unknowns. Then the following linear system of equations is solved:

$$JdX=-R\,, \tag{22}$$

where *dX* is an update to the vector of unknowns. After *dX* is calculated, the vector of unknowns *x* is updated according to:

$$X_{j+1}=X_j+dX_j\,, \tag{23}$$

where the subscript *j* refers to the iteration number. After the primary variables are updated, all secondary variables, such as the fluid properties, are updated. Then the residual vector is recalculated. Iteration is continued until the Euclidean and infinity norm of *R* and *dX* are below a convergence criterion.

2.2.7 Handling fracture aperture

Proppant is allowed to flow into or out of a fracture element only if the aperture of the element is greater than the proppant diameter.

To handle fracture closure, the upper part of aperture (above proppant bed) and the proppant bed are allowed to have different aperture. The aperture above the proppant bed, E_{upper}, is calculated in the same way described by McClure and Horne (2013). The proppant bed aperture, E_b, is subject to the following rule.

(1) If proppant bed is zero ($h_b = 0$), the bed and slurry apertures are set equal ($E_b = E_{upper}$).

(2) If the bed thickness is larger than the aperture of upper part of aperture ($E_{upper} \leq E_b$), the bed thickness is kept constant.

(3) If the bed thickness is smaller than the upper part of aperture ($E_{upper} \geq E_b$), the bed thickness is increased.

The bed thickness is updated explicitly, by holding its value constant and increasing it at the beginning of the next timestep. In order to assure convergence can be guaranteed by reducing timestep, the bed thickness is not permitted to grow faster than a certain rate. The rule is:

(1) If the upper part of the fracture is larger than the sum of the thickness and a user-defined maximum change of thickness ($E_{upper} > E_b + \Delta E_{b,\max}$), the maximum change is added to the thickness ($E_b = E_b + \Delta E_{b,\max}$).

(2) Otherwise, they are set equal ($E_b = E_{upper}$).

$\Delta E_{b,max}$ is determined as $\Delta E_{b,\max} = v_w dt$, where v_w is the widen rate, which is 10^{-3} m/s in this study.

3. RESULT AND DISCUSSION

To check that the calculation results are reasonable, we ran a simulation of a simple case with 1-D fracture geometry and did sensitivity analysis by changing 4 kinds of variables related to proppant. In future work, we will perform simulations for direct comparison against other published results and test in fracture network simulations.

3.1 Simulation with 1-D natural fracture

We performed a simple simulation to check conservation of mass for water and proppant. Figure 4 shows the fracture geometry. The blue line represents a preexisting fracture, and the black line represents the wellbore. The fracture was not permitted to propagate. In this simulation, twenty fracture elements were used. The length of the fracture was 40 m and the fracture height was 100 m. Slurry with 50 kg/m^3 proppant concentration was injected for about 10,000 seconds. The maximum fluid injection rate was set to 50 kg/s with a maximum injection pressure of 70 MPa. A 1-D leakoff model was used to calculate fluid leakoff from the fracture (Vinsome and Westerveld, 1980). Proppant density, proppant diameter, and proppant bed porosity were 1500 kg/m^3, 0.00084 m, and 0.44, respectively.

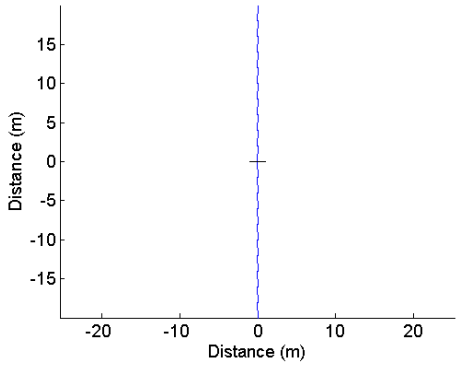

Figure 4: 1-D natural fracture with a well.

Figure 5 shows the simulation result at the end of the simulation. In Figure 5, "Eopen" represents the fluid volume stored per fracture surface area, including both the slurry region and the proppant bed. Table 1 shows the parameters used in the simulation. The parameters are well explained in McClure and Horne (2013).

Table 1:The parameters used in the simulations.

Parameter	*Value*	*Parameter*	*Value*
Constant for slurry viscosity(β)	*-2 [-]*	*Residual void aperture*	*0.5 [mm]*
Initial fluid pressure	*18 [Mpa]*	*Residual hydraulic aperture*	*0.002 [mm]*
Initial fluid density	*1000 [kg/m^3]*	*Fracture cohesion*	*0.5 [MPa]*
Fracture height (h)	*100 [m^3]*	*90% closure stress for void aperture*	*20 [MPa]*
Matrix permeability	*3,000 [nm^2]*	*90% closure stress for hydraulic aperture*	*20 [MPa]*
Water compressibility	*0.0004 [MPa^{-1}]*	*Water viscosity (μ_f)*	*1 [cp]*
Proppant concentration of injection fluid	*50 [kg/m^3]*	*Radiation damping coefficient (η)*	*3.0 [MPa/(m/s)]*
Proppant density	*1500 [kg/m^3]*	*Shear dilation angle for hydraulic aperture*	*2.0 [°]*
Proppant diameter	*0.84 [mm]*	*Maximum injection rate*	*50 [kg/s]*
Maximum proppant bed porosity ($\phi_{b,max}$)	*0.44 [-]*	*Maximum injection pressure*	*70 [MPa]*
Porosity compressibility ($C_{\phi b}$)	*0 .00145 [MPa^{-1}]*	*Wellbore volume (V_{well})*	*94.2478 [m^3]*

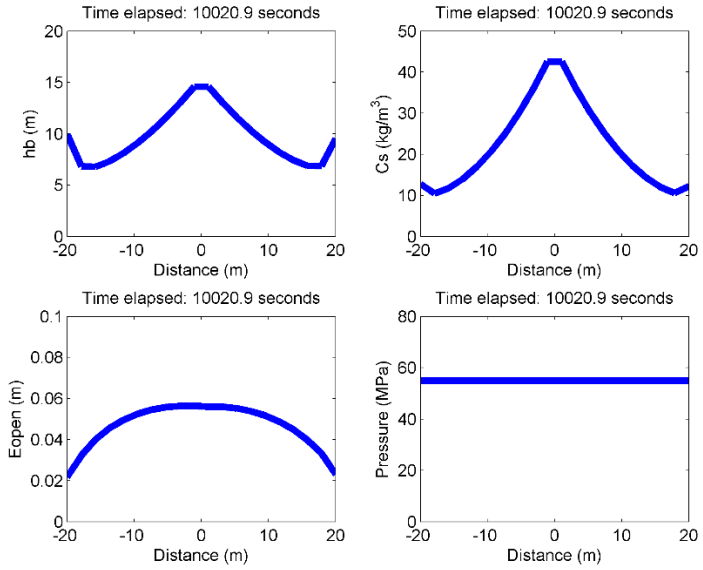

Figure 5: The result of 1-D natural fracture with leak off. The horizontal axis is distance along the fracture. The wellbore is located at distance is zero. The values in the wellbore element are not shown in the graph.

Figure 6 and 7 show the results of a global mass balance calculation on water and proppant. The global mass balance is performed by calculating the total mass of fluid or proppant in the fractures and the wellbore and subtracting the initial amount of fluid or proppant in the fractures and the wellbore and also subtracting the total volume of fluid and proppant injected from the surface. The deviation from zero is the global mass balance error

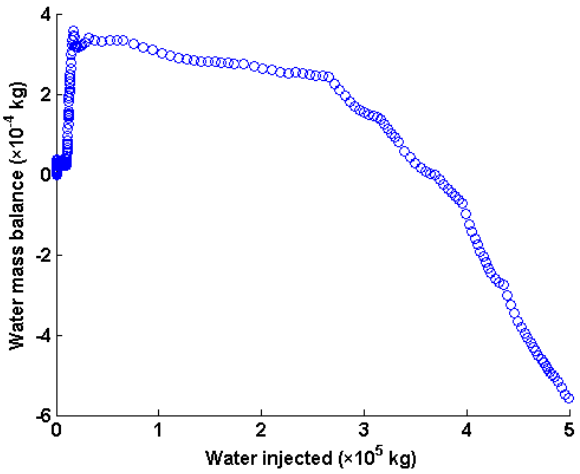

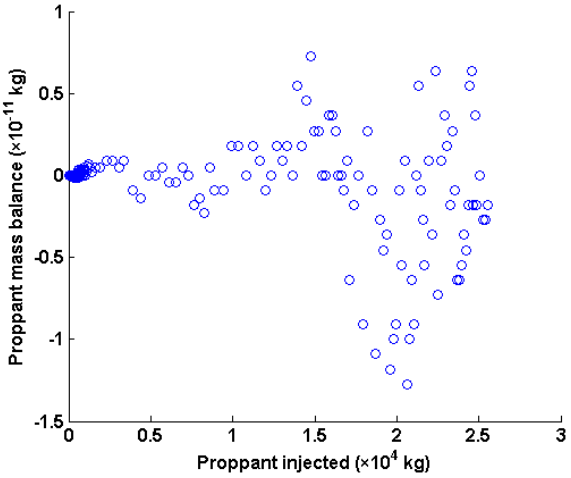

Figure 6: Water mass balance (left).

Figure 7: Proppant mass balance (right).

3.2 Sensitivity Analysis

A sensitivity analysis was conducted by changing four variables: proppant concentration in injection fluid, proppant density, proppant diameter, and proppant bed porosity. The fracture geometry was the same as in Section 3.1, and similarly, the fracture was not permitted to propagate. Table 2 shows the settings used in the simulations. Figures 9 - 12 show the results of the simulations.

Table 2: The settings of performed simulations.

Simulation number	*Proppant concentration in injection fluid [kg/m³]*	*Proppant density [kg/m³]*	*proppant diameter [m]*	*Maximum proppant bed porosity [-]*
1-1	*50*	*1500 (ρ_p/ρ_f=1.5)*	*0.00084 (Mesh 20/40)*	*0.44 (Very loose random packing)*
1-2	*100*			
1-3	*150*			
2-1	*100*	*2000 (ρ_p/ρ_f=2.0)*	*0.00084*	*0.44*
2-2		*2500 ($\rho_p/\rho f$=2.5)*		
2-3		*3000 (ρ_p/ρ_f=3.0)*		
3-1	*100*	*1500*	*0.00021 (Mesh 70/140)*	*0.44*
3-2			*0.0015 (Mesh 10/20)*	
3-3			*0.00238 (Mesh 8/12)*	
4-1	*100*	*1500*	*0.00084*	*0.26 (Thickest regular packing)*
4-2				*0.36 (Close random packing)*
4-3				*0.4764 (Thinnest regular packing)*

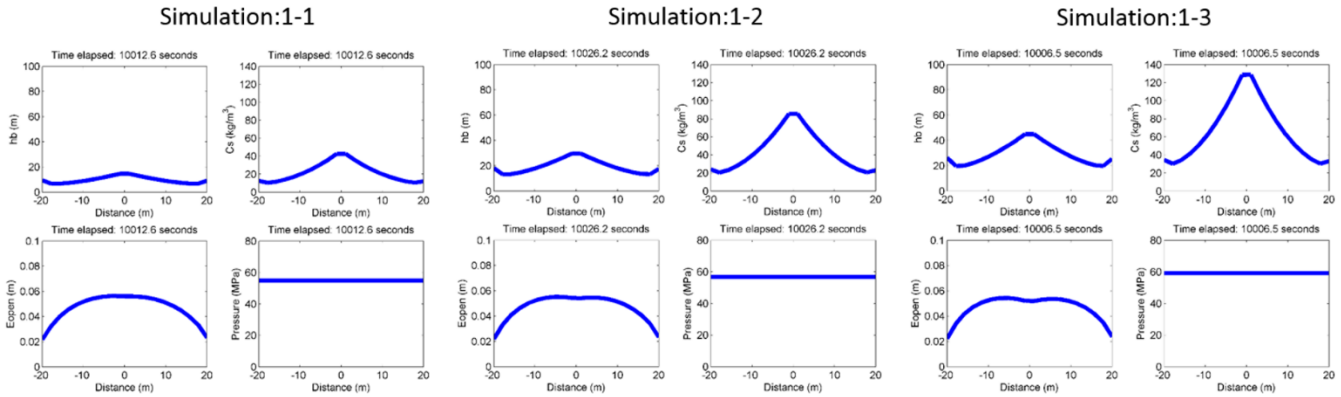

Figure 8: Simulation results with different proppant concentration in the injection fluid.

As seen from Figure 8, as proppant concentration in injection fluid increased, the proppant concentration in fracture and proppant bed height increased, which is physically reasonable.

Figure 9 shows the result when the proppant density was changed. Both the concentration and bed height at the fracture tips were higher when the proppant density was lower because lighter grains settled into the proppant bed more slowly.

Figure 10 shows the effect of changing proppant diameter. As seen in Equation 17, the settling velocity is a function of proppant diameter, and therefore proppant bed height is greater when proppant diameter is larger.

Figure 11 shows the effect of changing the porosity of the proppant bed. The proppant bed is higher when porosity is larger because the same mass of proppant takes up more space in the proppant bed.

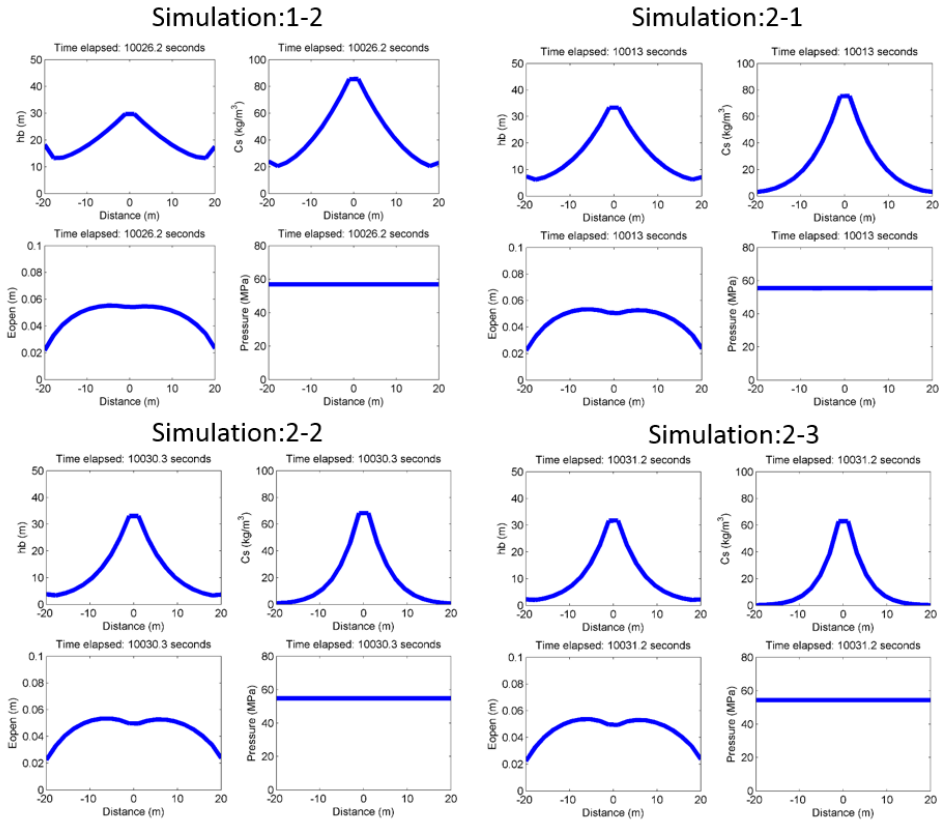

Figure 9: Simulation results with different proppant density.

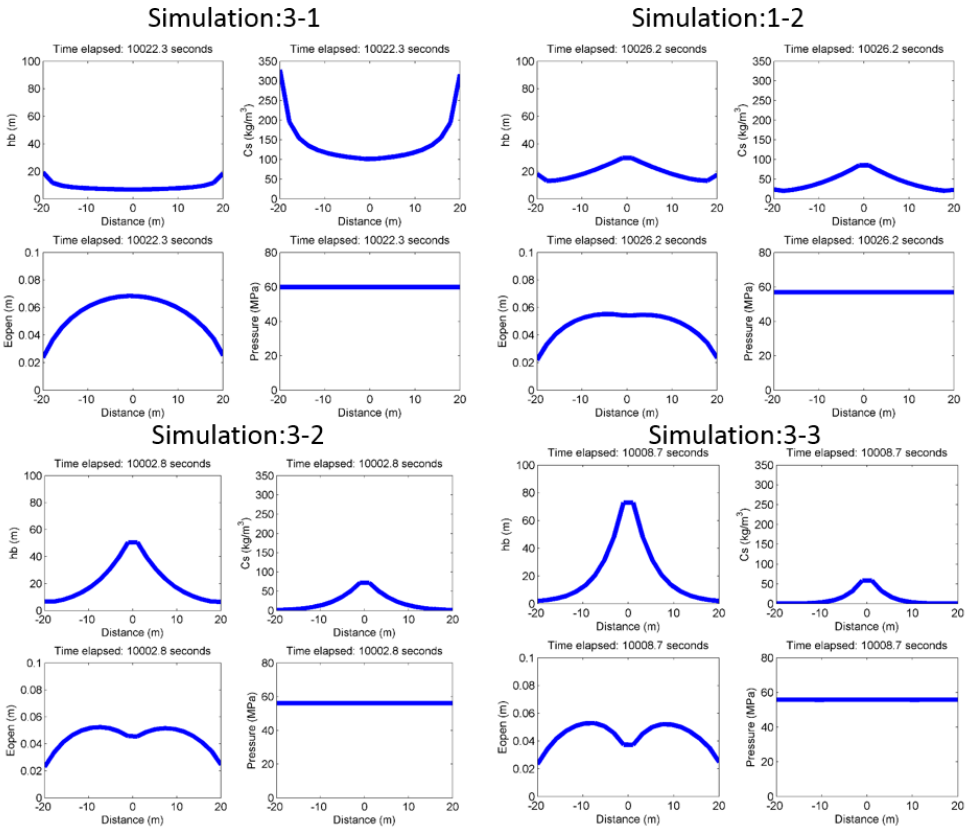

Figure 10: Simulation results with different proppant diameter.

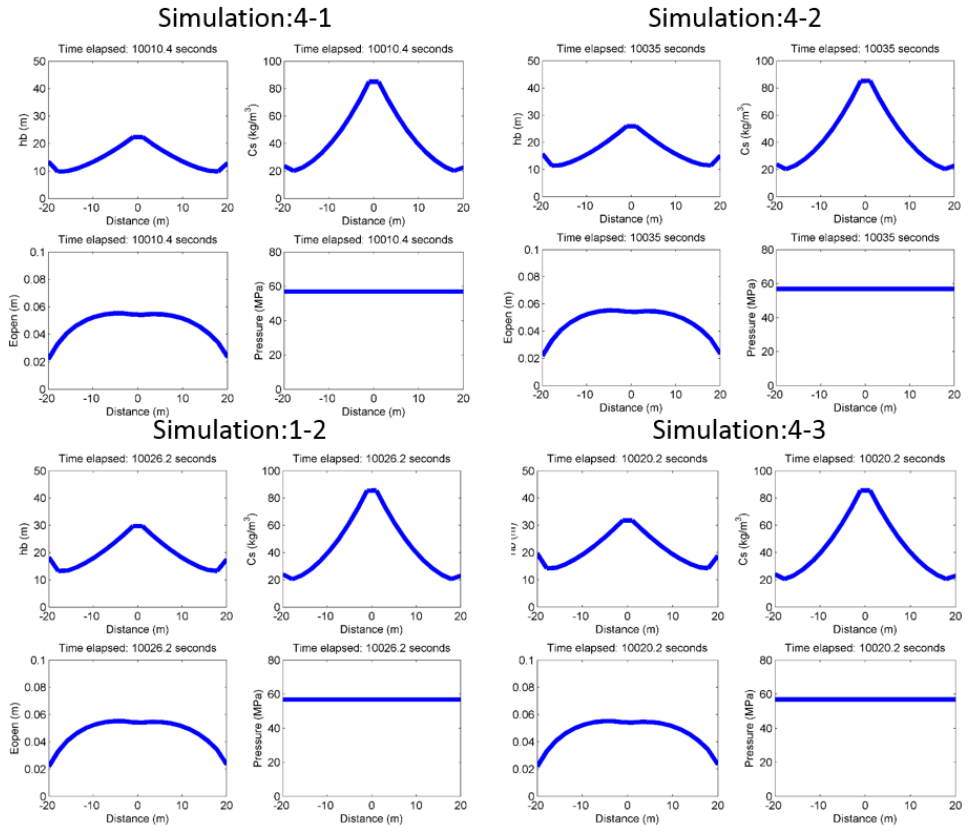

Figure 11: Simulation results with a variable of the proppant bed porosity.

4. CONCLUSION

The ability to model proppant transport was added into CFRAC, a discrete fracture network simulator that fully couples fluid flow with the stresses induced by fracture deformation. We ran validation simulations to confirm that the code conserves mass for water and proppant and to perform sensitivity analysis to confirm that the simulation results are physically plausible.

ACKNOWLEDGEMENTS

Thank you to Weatherford for supporting this study.

REFERENCES

Adachi, J., Siebrits, E., Perce, A., and Desroches, J.: Computer simulation of hydraulic fractures, *Int. J. Rock Mech. Min. Sci.* **44,** (2007) 739-757.

Crouch, S.L., Starfield, A.M.: Boundary element methods in solid mechanics: with applications in rock mechanics and geological engineering, Allen and Unwin, London Boston (1983).

Dontsov, E.V. and Peirce, A.P.: Slurry flow, gravitational settling and a proppant transport model for hydraulic fractures, *J. Fluid Mech.* **760**, (2014), 567-590.

Gadde, P.B., Liu, Y., Norman, J., Bonnecaze, R., and Sharma, M.M.: Modeling Proppant Settling in Water-Fracs, *Proceedings*, the SPE Annual Technical Conference and Exhibition, Houston, TX (2004).

Jaeger, J.C., Cook, N.G.W., Zimmerman, R.W.: Fundamental of Rock Mechanics, 4th edn. Blackwell Pub, Malden (2007).

Kim, J., Tchelepi, H., Juanes, R.: Stability, accuracy, and efficiency of sequential methods for coupled flow and geomechanics, *SPE J.* **9**(2), (2004), 227-236.

Li, T., Shiozawa, S., and McClure, M.: Thermal breakthrough calculations to optimize design of a multiple-stage Enhanced Geothermal System, *Proceedings*, Geothermal Resource Council Transactions, **38** (2014).

Mack, M., Sun, J., and Khadikar, C.: Quantifying Proppant Transport in Thin Fluids – Theory and Experiments, *Proceedings*, the SPE Hydraulic Fracturing Technology Conference, Woodlands, TX (2014).

McClure, M.W.: Modeling and Characterization of Hydraulic Stimulation and Induced Seismicity in Geothermal and Shale Gas Reservoirs, Stanford University, CA (2012).

McClure, M.W., Roland, N.H.: Discrete Fracture Network Modeling of Hydraulic Stimulation: Coupling Flow and Geomechanics, SpringerBriefs in EarthSciences, Springer (2013).

McClure, M.W., Roland, N.H.: An investigation of stimulation mechanisms in Enhanced Geothermal Systems, *Int. J. Rock Mech. Min. Sci.* **78**, (2014), 242-260.

McClure, M.W., Babazadeh, M., Shiozawa, S., and Huang, J.: Fully Coupled Hydromechanical Simulation of Hydraulic Fracturing in Three-Dimensional Discrete Fracture Network, *Proceedings*, SPE 173354-MS, the SPE Hydraulic Fracturing Technology Conference, Woodlands, TX (2015).

McGhee, T.J.: Water Resourced and Environmental Engineering, Sixth Edition, McGraw-Hill, New York, 1956.

Mobbs, A.T. and Hammond, P.S.: Computer Simulations of Proppant Transport in a Hydraulic Fracture, *SPE Production & Facilities J.* **16**(2), (2001), 112-121.

Rice, J. R.: Spatio-temporal complexity of slip on a fault, *Journal of Geophysical Research*, **98**(B6), (1993), 9885-9907, doi:10.1029/93JB00191.

Shiozawa, S., and McClure, M.: EGS designs with Horizontal Wells, Multiple Stages, and Proppant, *Proceedings*, 39th Workshop on Geothermal Reservoir Engineering, Stanford University, Stanford, CA (2014).

Shou, K.J., and Crouch, S.L.: A higher order Displacement Discontinuity Method for analysis of crack problems. *Int. J. Rock Mech. Min. Sci. Geomech. Abstr*. **32**(1), (1995), 49-55.

Vinsome, P. K., and Westerveld, J.: A simple method for predicting cap and base rock heat loses in thermal reservoir simulators, *Journal of Canadian Petroleum Technology*, **19**(3), (1980), *87-90.*

Wang, J., Joseph, D.D., Patankar, N.A., Conway, and M., Barree, R.D.: Bi-power law correlations for sediment transport in pressure driven channel flows, *Int. J. Multiphase Flow* **29**, (2003), 475-594.